Spatial V2X Traffic Density Channel Characterization for Urban Environments

Fausto Granda, *Student Member, IEEE*, Leyre Azpilicueta, *Member, IEEE*, Mikel Celaya-Echarri, *Student Member, IEEE*, Peio Lopez-Iturri, *Member, IEEE*, Cesar Vargas-Rosales, *Senior Member, IEEE*, and Francisco Falcone, *Senior Member, IEEE*

***Abstract*— In this work, Vehicle-to-everything (V2X) wireless communications performance is analyzed, in order to account for inherent scenario complexity, in the deployment phase of wireless systems towards the implementation of a Context Aware environment. An urban environment has been simulated by means of an in-house three-dimensional (3D) Ray Launching algorithm, coupled with a microscopic vehicular movement simulator, accounting for embedded urban elements as well as variable traffic densities within the complex environment. Large-scale and small-scale results are presented, as well as statistical analysis of the impact of different traffic densities. A campaign of measurements in the same real scenario has been performed, showing good agreement with wireless channel estimations for the considered frequency. These results can aid in V2X deployment configurations in urban environments, in order to minimize power consumption, optimize interference levels and increase overall system performance.**

***Index Terms*— V2X traffic density, channel characterization, urban environments, 3D ray Launching, microscopic vehicular simulator.**

I. Introduction

VEHICLE-TO-VEHICLE (V2V) and Vehicle-to-Infrastructure (V2I) communications are attracting important attention from academia [1], vehicle industry [2] and Government regulations [3], as they improve safety and facilitate cooperative driving. In 1999, the U.S. Federal Communications Commission (FCC) allocated 75 MHz of licensed spectrum at 5.9 GHz to be used for V2V and V2I communications known as Dedicated Short-Range Communications (DSRC). Besides, the IEEE 802.11p standard [4], part of the Wireless Access in Vehicular Environments (WAVE) initiative [5], was developed to operate at this frequency band. The IEEE 802.11p standard, which includes Physical (PHY) and Medium Access Control (MAC) layer specifications, allows to directly transmit and receive messages without the need for exchanging control sequences before, which guarantees low latency and reduces the message overhead, however, some studies show that communications based on IEEE 802.11p face some issues such as, short-lived V2I connections, lack of quality-of-service (QoS) guarantee and increase in the packet delay, resulting in undesirable performance under harsh vehicular environments [6]. Harsh vehicular environments are related to high levels of Vehicular Traffic Density (VTD), which has been increasing due to factors such as increased motorization, badly managed roads or poorly designed intersections, among others. High levels of VTD increase air pollution, fuel consumption and commuting time, with the resulting inefficient transportation service and frustration of travelers. Although Intelligent Transportation Systems (ITS) based solutions have been offering several non-intrusive technologies based on laser, ultrasound, radar, multimedia signals [7], and wireless connectivity to monitoring the traffic evolution, yet the impact and implications of VTD on vehicular propagation channels is a research area that requires attention.

Vehicular channels exhibit rapid temporal variability and inherent non-stationarity, and vehicular communications channel propagation characteristics are one of the most fundamental differentiating factors when compared with other types of wireless systems, [8]. For instance, the urban radio channel system design for vehicular communication faces many challenges because its highly dynamic in nature, where variable vehicular factors such as speed, volume, density, relative geometries that result in sudden changes between Line of Sight (LoS), Non Line of Sight (NLoS) and Quasi Line of Sight (QLoS) conditions, and different roadside environments, make the V2V and V2I channels significantly different from other channel characterizations (e.g., cellular networks) and give rise to issues such as: temporal and spatial variations of path loss, multipath effects, polarization mismatch, impairments of the PHY layer performance [9], etc.

Manuscript received April 29, 2019; revised November 2, 2019; accepted January 24, 2020. Date of publication February 26, 2020; date of current version May 3, 2021. This work was supported in part by the SEP-CONACyT Research Project under Grant 255387, in part by the School of Engineering and Sciences, in part by the Telecommunications and Networks Research Group, Tecnologico de Monterrey, and in part by the Departamento de Electrica, Electronica y Telecomunicaciones, Universidad de las Fuerzas Armadas ESPE. The Associate Editor for this article was G. Ostermayer. *(Corresponding author: Leyre Azpilicueta.)*

Fausto Granda is with the Electrical and Electronic Engineering Department, Universidad de las Fuerzas Armadas ESPE, Sangolquí 171-5-231B, Ecuador.

Leyre Azpilicueta, Mikel Celaya-Echarri, and Cesar Vargas-Rosales are with the School of Engineering and Sciences, Tecnologico de Monterrey, Monterrey 64849, Mexico (e-mail: leyre.azpilicueta@tec.mx).

Peio Lopez-Iturri and Francisco Falcone are with the Electrical and Electronic Engineering Department, Universidad Pública de Navarra (UPNA), 31006 Pamplona, Spain.

Digital Object Identifier 10.1109/TITS.2020.2974692

Channel modeling approaches can be roughly classified into three categories: (1) empirical, (2) geometry-based deterministic models (GBDMs), and (3) stochastic models, which in turn can be classified as non-geometrical stochastic models (NGSMs) and geometry-based stochastic models (GBSMs). While empirical tests provide useful insight for specific in situ scenarios, [10], and NGSMs/GBSMs could fail to characterize significant surrounding obstacles, the GBDMs approaches are suited for vehicular propagation analysis of urban scenarios yielding a reasonable tradeoff between accuracy and computational cost [11].

Some current state-of-the art simulators focus mainly on vehicular communications based on NGSMs/GBSMs, and although the literature includes many propagation models and channel simulators for V2V systems [12], [13] and V2I [14], [15], there is a need for further studies to investigate the channel propagation using three-dimensional GBDMs tools in urban environments. Despite a plentiful research work related to VTD estimation, using different techniques (e.g., unsupervised clustering schemes with Hidden Markov models [16] or cumulative road acoustics [7]), there is still a need for deterministic channel models facilitating realistic analysis of the VTD impact on the V2V and V2I Urban Radio Propagation Channel (URPC).

Related information of the VTD impact on V2V urban environments is presented in [17], where it is shown that VTD significantly affects the channel statistics especially for small spatial scale scenarios (transmitter (TX)- receiver (RX) distance is smaller than 300 m) where the smaller the TX-RX distance, the larger impact of the VTD. In [18], channel measurements and stochastic modeling for V2V show higher values of root mean square delay spread for high-density traffic, where fading tap amplitudes were modeled using Weibull distribution. In [19], the impact of VTD on mobile-to-mobile (M2M) Ricean fading channel is analyzed. Results suggest that VTD significantly affects both the shape and value of the Doppler power spectral density (PSD) and correlation function (CF). The Doppler PSD tends to be more evenly distributed across all Doppler frequencies with a higher VTD. With a low VTD, the received power from the LoS component may be significant, while the power from the moving cars may be small. The effect of the radio channel is highly influenced by the rich scattering environment under high traffic congestion, and most important scatters are traffic signs, trucks, and bridges, whereas other cars do not significantly contribute to the multipath propagation according to [20].

The VTD also impacts the network layer. In [14], it is demonstrated that high traffic density with heavy machinery/trucks, are related with significant reduction on the V2I reliable connectivity range and increase in the communications link variability, which is confirmed in [21] where the results show that increasing traffic density keeps the relationship with increased interference and increase in the update delay (UD), a performance metric for collision avoidance. Under smaller vehicle densities, the IEEE 802.11p standard offers end-to-end delays of less than 100 ms and throughputs equivalent to 10 kbit/s which satisfy the requirements posed by active road safety applications, [22]. High user densities can cause network scalability issues due to the related interference affecting metrics such as reliability, [23].

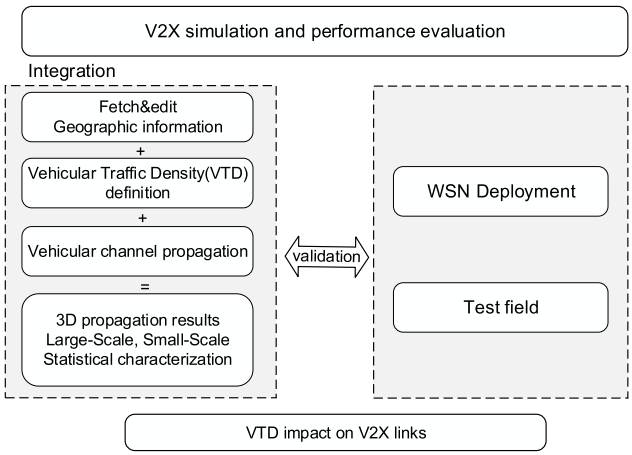

Fig. 1. Approach of the paper organization.

In this work, a GBDM approach based on an in-house three dimensional (3D) ray-launching (RL) algorithm (3D-RL), coupled with a microscopic vehicular movement simulator SUMO [24] have been used to analyze the impact of the VTD on V2V and V2I channel statistics in an urban scenario. Spatial TX-RX distance/position and segmentation considerations were used to analyze homogeneous clusters of information to identify differences in the large-scale and small-scale statistics caused by the variation of the vehicle's density in the scenario given the non-stationary nature of the vehicular communications channel, [25]. The use of a ray-launching based algorithm is given by the fact that it can provide general coverage/capacity estimations, including zone coverage calculations, enabling the analysis of multiple communication link types [26], [27].

Fig. 1 illustrates a schematic diagram of the followed procedure. The geographic information of the scenario fetched from OpenStreetMap (OSM) [28], a free database, is represented in a microscopic vehicular traffic simulator where different VTD are generated. The resulted vehicular behavior is integrated with a 3D-RL channel propagation simulator to obtain channel propagation results under different VTD levels, for V2I and V2V. These integrated results were processed to understand the large-scale, Small-Scale and statistical implications of the VTD. Finally, a measurement campaign, using WSN (Wireless Sensor Network) nodes were performed to validate its findings with the aforementioned simulated results.

This work is oriented to complement some existing contributions summarized in Table I related to RL and microscopic vehicular integration for the analysis of the VTD impact on URPC.

In [18], the authors presented an analysis of the VTD influence on the channel statistics for V2V using a stochastic channel modeling and comparing it with test-field measurements. In [29], [30] and [31], it is proposed an integrated simulator (channel propagation and microscopic vehicular) for Vehicle-to-everything (V2X = communications with some channel propagation measurements as received signal strength (RSS), power delay profile (PDP), packet error rate (PER), however the impact of the VTD is not tackled. Two main

TABLE I
CONTRIBUTIONS OF RAY LAUNCHING AND MICROSCOPIC VEHICULAR INTEGRATION FOR V2X

Ref.	Channel modeling approach	Vehicular movement approach	Propagation Channel Simulations/Measurements
[18]	Stochastic	Measurements	Delay spread, amplitude statistics, and correlations for V2V (VTD influence).
[29]	3D-RL	SUMO	N.A.
[30]	3D-RL	SUMO	PDP, PER
[31]	2.5D-RL GEMV2	SUMO	Received signal strength, packet delivery ratio, reliable communication range
This work	3D-RL	SUMO	Large-scale path loss, RSS statistics, Doppler profile, Doppler shift, VTD influence, statistical characterization.

N.A.: Not available, PDP: power delay profile, EV's: Eigenvalue distributions. PER: Packet error rate.

contributions of the presented work are the following: a) the use of spatial and segmentation considerations which can lead to more fine-grained large-scale and small-scale information, useful for detailed measurements and statistical analysis for a better understanding of the impact of the VTD on V2V and V2I channel characterization, and b) the integration of accurate simulation tools such as geographical database, 3D-RL algorithm, and microscopic vehicular simulator as a contribution for federated approaches recommended in [32].

The remaining parts of the paper are organized as follows: Section II describes the theoretical basis, detailed integration of the used simulation tools, the configuration and spatial considerations of the scenario and the representation of the VTD. Section III describes the large-scale and small-scale simulation results. Statistical analysis of VTD on V2X links is set out in Section IV while Section V presents a campaign of measurements and the algorithm validation. Finally, the conclusions are presented in Section VI.

II. WIRELESS CHANNEL CHARACTERIZATION

A. Ray Launching Technique

An in-house 3D-RL algorithm has been developed based on Geometrical Optics (GO) approach and the Uniform Theory of Diffraction (UTD). The principle of RL approaches is that a consistent number of rays follow a path from the transmitter to the receiver over the direct, reflected and diffracted rays according to geometric considerations and geometrical optics rules. The resulting complex impulse response incorporates the complete channel information. These methods require a detailed description of site-specific propagation environments. Some shadowing problems are caused by applying GO due to field prediction impairments in edges and discontinuities areas. These problems are solved in the algorithm by introducing diffraction phenomenon based on UTD. In that sense, the diffraction coefficients on the edges of the diffractive elements have been considered to predict the shadowing areas' field. The electric field E created by GO and the diffracted electric field created by UTD are calculated by [33]

$$E_{\mathrm{GO}}^{\perp\parallel} = \sqrt{\frac{P_{\mathrm{rad}} D_{\mathrm{t}}(\theta_{\mathrm{t}}, \emptyset_{\mathrm{t}})\eta_0}{2\Pi}} \frac{e^{-\mathrm{j}\beta_0 r}}{\mathrm{r}} \mathrm{X}^{\perp\parallel} L^{\perp\parallel} \tag{1}$$

$$E_{\mathrm{UTD}}^{\perp\parallel} = e_0 \frac{e^{-\mathrm{j}ks_1}}{s_1} D^{\perp\parallel} \sqrt{\frac{s_1}{s_2(s_1+s_2)}} e^{-\mathrm{j}ks_2} \tag{2}$$

where $\beta_0 = 2\pi f_{\mathrm{c}}\sqrt{\varepsilon_0\mu_0}$, $\varepsilon_0 = 8.854 \cdot 10^{-12}$F/m, $\mu_0 = 4\pi \cdot 10^{-7}$H/m and $\eta_0 = 120\pi$ ohms. P_{rad} is the radiated power of the transmitter antenna. $D_{\mathrm{t}}(\theta_{\mathrm{t}}, \emptyset_{\mathrm{t}})$ is the directivity where rays are launched as defined in the spherical coordinate system at an elevation angle θ_{t} and an azimuth angle ϕ_{t}. $\mathrm{X}^{\perp\parallel}$ and $L^{\perp\parallel}$ are the polarization ratio and path loss coefficients for each polarization, r the distance in the free space and f_{c} the transmission frequency. In equation (2), $D^{\perp\parallel}$ are the diffraction coefficients for each polarization and s_1, s_2 are the distances from the source to the edge and from the edge to the receiver point.

In the literature, the in-house developed 3D-RL code has been validated to predict wireless propagation in complex environments [13]. Also, it has been shown that the basis of GO/UTD predicts accurately wireless communication propagation when a complete 3D scenario is taken into account [34].

B. OSM, JOSM, SUMO

OpenStreetMap (OSM) is a collaborative project to create a free editable map of the and is one of the most popular examples of volunteered geographic information (VGI). Java OpenStreetMap editor (JOSM) [35] is an open-source extensible editor for OpenStreetMap for Java and allows to edit the OSM data (nodes, ways, and relations) and their metadata tags [36].

Simulation of Urban Mobility (SUMO) [24], is an open-source, microscopic, space-continuous, multi-modal traffic simulator based on the microscopic car following model developed by Stefan Krauß in 1998 [37], which keeps some similarities with the car-following model presented by Gibbs in 1981 [38]. Microscopic means that vehicles are modeled explicitly, have an own route and move individually through the network according to a realistic mobility model. Simulations are deterministic by default but there are various options for introducing randomness. The model uses restriction parameters like the maximum acceleration and deceleration, maximum velocity, length of the vehicle, and driver's imperfection in holding the safe velocity, [37]. SUMO has been extensively applied in different projects related to network performance, traffic assignment, vehicle routing, traffic analysis [39], traffic emission, V2X [40] and other diverse traffic issues.

C. 3D-RL and Vehicular Mobility Integration

In the presented work, for the simulation of the V2X (V2I, V2V, I2V) radio propagation phenomenon, the integration of tools such as geographic information, 3D-RL, and microscopic vehicle movement simulator has been done. Even though the 3D-RL algorithm can represent the vehicular movement for V2X purposes, yet the vehicular density requires a more accurate representation that 3D-RL is unable to perform. In this

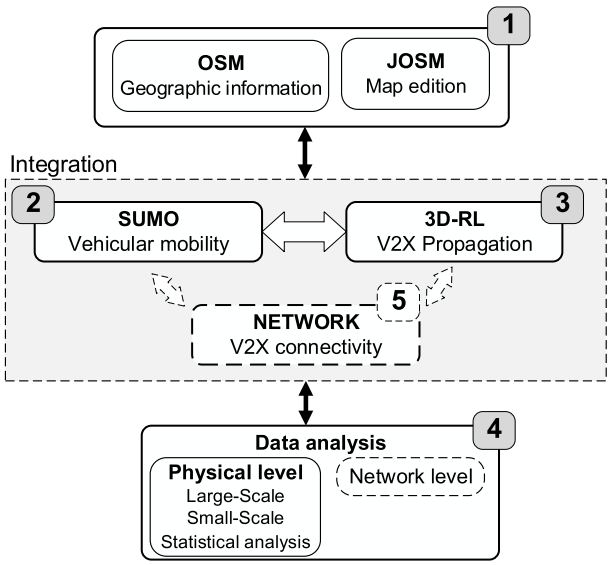

Fig. 2. Schematic solution approach.

way, 3D-RL and SUMO were joined to present integrated results for analysis. Fig. 2 illustrates the solution approach which includes four stages: 1) the scenario selection and edition, 2) the VTD and movement configuration, 3) the 3D-RL propagation simulation and, 4) the VTD analysis. Stage 5 is considered for future integration with network layer modules as a part of a five-stage top-down methodology for building realistic simulation scenarios, suitable for multiple levels of abstraction in V2X simulations.

In stage 1, the geographic information of the urban scenario is obtained and exported from OSM, which coordinate system World Geodetic System (WGS) [41] needs to be pre-processed to be compatible with SUMO, that needs Cartesian coordinates (meters). The geographic information from OSM is edited in JOSM were useless geo-referencing information, non-relevant routes and places are eliminated and some parameters as velocity limit, lane number, type of lane (i.e., highway, residential), lane direction, and axis translations useful for SUMO and 3D-RL compatibility are configured.

In stage 2, the vehicle movement and density parametrization are simulated. The traffic-stream parameters, fall into two broad categories: macroscopic parameters (volume or rate of flow, speed, and density) characterize the traffic stream as a whole, and microscopic parameters (spacing and time headway) characterize the behavior of individual vehicles in the traffic stream [42]. In this stage, the vehicle movement is defined by the default car following model configured in SUMO. The density, a macroscopic measure of traffic stream conditions, is defined as the number of vehicles occupying a given length of highway or lane and is generally expressed in vehicles per mile (vpm) or vehicles per mile per lane (vpmpl). Density is difficult to measure directly, and it is perhaps the most important of the three traffic-stream parameters because it is the measure most directly related to traffic demand. Parameters such as vehicle routes, vehicle type, maximum speed, initial and final position, depart and arrive lane, start and final time, vehicles per hour, traffic lights parameters, etc., are configured to obtain three vehicular densities: High Density (HD), Medium Density (MD) and Low Density (LD).

TABLE II
SCENARIO REFERENCES

Description	Position (x, y, z) [m]
AV-1 /AV-2	(x, 93, 0) / (x, 82, 0)
ST-1/ ST-2/ ST-3	(x, 39, 0) / (103, y, 0) / (180, y, 0)
TX1 / TX2	(164, 78, 3.5) / (114, 43, 3.5)
C1 / C2 / C3	(118, 80, 1.5), (171, 35, 1.5), (100, 53, 1.5)
C4	(115, 85, 1.5)

TX1, TX2 = Transmitters antennas on lampposts
C1, C2, C3 = Transmitters antennas on cars.
C4 = Reference point for Power delay profile measurements.

In stage 3, propagation simulation using the 3D-RL software is performed. From mixed information of OSM, JOSM, and SUMO, the 3D scenario is parametrized and created into the 3D-RL simulator, where the Cartesian coordinates (x, y) are matched with JOSM and SUMO, while the Cartesian coordinate (z) is matched with OSM. The in-house 3D-RL algorithm divides the represented 3D urban scenario in several cuboids of a fixed size. The main pieces of information stored in each cuboid that the ray passes in its trajectory are PDP and Doppler profile (DP) [43]. From PDP is extracted the RSS, which is synonymous with theoretical P_r(power received) defined in the Friis transmission formula [44] however, we used RSS to discern the 3D-RL simulation results from theoretical calculations. Parameters such as frequency of operation, the radiation pattern of the antennas, number of multipath reflections, separation angle between rays and cuboids dimension, can be configured in the algorithm. The material properties of the scenario were considered with the conductivity and relative permittivity at the frequency range of operation of the system under analysis.

D. Urban Scenario Description

Fig. 3(a) displays a 2D aerial-view of the modeled urban scenario, an approximate replica of Plaza de Gongora (WGS84 Latitude/Longitude: 42.79793, -1.63921), located in Pamplona, Spain. The Cartesian coordinates (x, y, z) of interest points are identified according to their relative position from the origin (0, 0, 0), presented in Table II. Fig. 3(b) depicts a 3D rendered aerial view of the scenario, where dimensions are shown (260 m x 120 m x 20 m) together with typical elements of an urban environment, such as buildings, vehicles, trees, benches, people, and lampposts. Fig. 3(c) shows the real scenario.

Due to power limitations of the equipment used in the measurement campaign (see section V), the transmit power simulated and configured, was set up at 0 dBm for both, V2V and V2I links, even when is natural to assume that the power of the transmitter antenna on the lampposts (V2I) shall be higher than the transmitter antenna of the cars (V2V). Simulation parameters are summarized in Table III.

The received signal threshold (RST) was chosen according to the minimum sensitivity information reported for some V2X (IEEE 802.11p) radio-communications commercial products, [45], [46], [47].

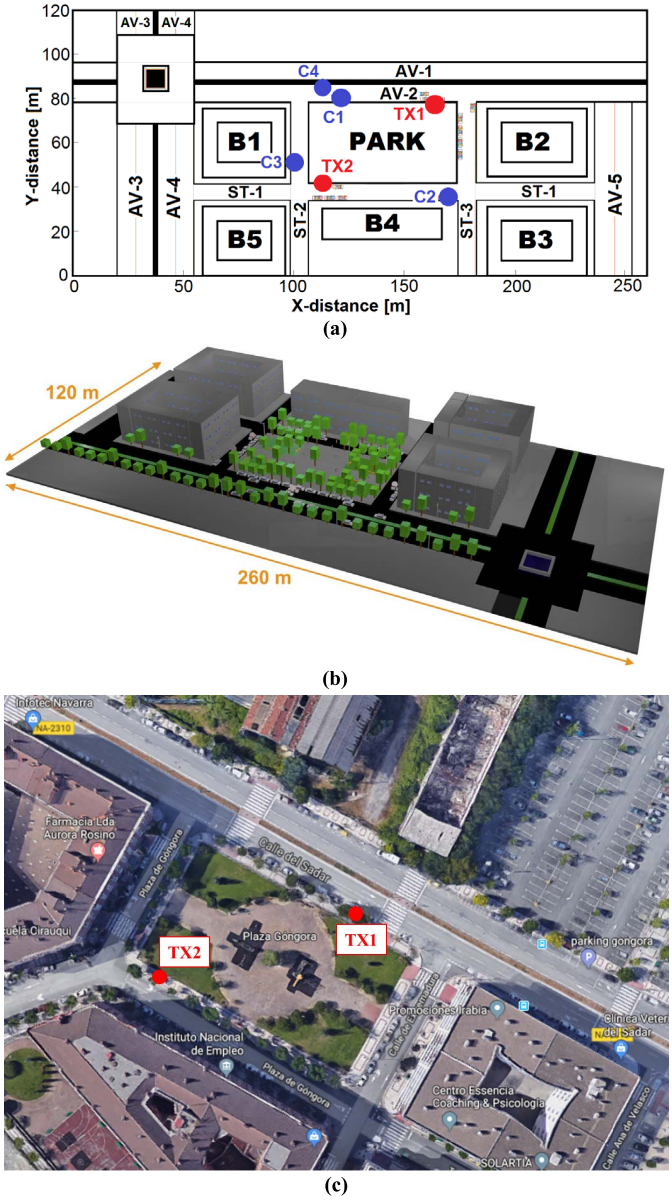

Fig. 3. Urban scenario: (a) 2D schematic view, (b) 3D schematic view, (c) Real view from Google Maps.

The VTD was calculated considering two parameters: the total simulated vehicles in the scenario at specific SUMO step time versus the full scenario capacity, this is when all the roads are occupied. Approximately 30% of scenario occupancy is considered for LD, while 50% and 80% are considered for MD and HD respectively. The Full Scenario Occupancy (FSO) was calculated as follows,

$$FSO[\text{vehicles}] = \frac{Total\ routes\ length\ [m]}{Vehicles\_length\ [m] + minGap[m]} \quad (3)$$

where

routes length [m] = Total length of the vehicular routes,
vehicles_length [m] = 5.0 m (default SUMO),
minGap [m] = 2.5 m, empty space after leader.

The largest routes are AV-1 and AV-2 with capacity for 58 passenger vehicles each one (see III for reference). When all the routes are fully occupied, a total of 270 vehicles are simulated simultaneously as is registered in Table IV.

TABLE III
SIMULATION PARAMETERS

Parameters	Values
TX1, TX2: Height **C1, C2, C3**: Height P_t */Gain(G_t)/Frequency / /Radiation pattern.	3.5 m 1.5 m 0 dBm/0 dB/5.9 GHz /omnidirectional.
RX: RST **/Gain(G_r)/Frequency /Height/ Radiation pattern.	−100 dBm/0 dB/5.9 GHz /1.5 m / omnidirectional.
3D-RL: horizontal and vertical angular resolution Angular resolution of diffracted rays. Maximum permitted reflections. Cuboid segmentation for analysis.	π/180 rad π/20 rad 7 hops 1 m^3 (1 m × 1 m × 1 m)

Pt *: Transmit power, RST ** (Received Signal Threshold).

TABLE IV
VEHICULAR TRAFFIC DENSITY DEFINITION

Route	Total length [m]	Full occupancy [total vehicles]
AV-1 (2 lanes)	453.60	58
AV-2 (2 lanes)	452.44	58
AV-3 (2 lanes)	180.86	22
AV-4 (2 lanes)	181.20	22
AV-5 (2 lanes)	165.34	20
ST-1 (2 lanes)	273.98	34
ST-2 (2 lanes)	85.80	10
ST-3 (2 lanes)	164.30	20
Roundabout (2 lanes)	203.74	26
Scenario	**2161.26**	**270**

Fig. 4(a) shows the VTD evolution during a SUMO step time span of 2100 s, for LD, MD and HD. For example, approximately 220 cars were simulated in the scenario for HD, while 90 cars for LD. Occupancy level at 100% were simulated with significant increase in the simulation time. Fig. 4(b) depicts a 2D view of the SUMO simulation for HD (220 cars, 80% occupancy, step time of 1253 s). Alternative VTD definition could be used as is presented in [7], where the density is defined by the vehicle's mean velocity: free-flow (0-10 km/h), medium-flow (10-40 km/h), jammed (above 40 km/h). There is an inverse relationship between density and velocity.

III. RESULTS

With the integrated information results from stage 3 previously described, large-scale parameters such as RSS, and small-scale parameters such as coherence bandwidth (B_C), root mean square delay spread (τ_{rms}) and Mean Excess Delay (τ_{mean}) can be calculated. The frequency dispersive effects due to the vehicle's movement can be also analyzed using the Doppler shift and Doppler spread parameters, for different vehicular velocities and frequencies.

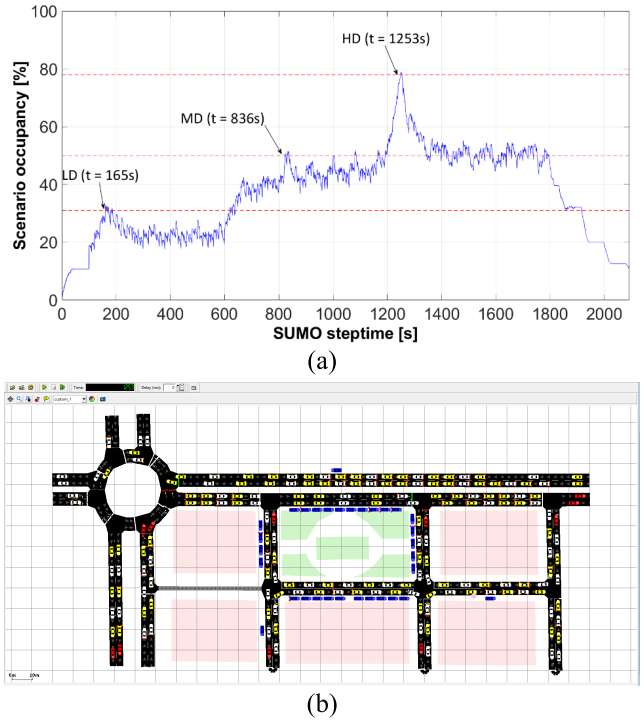

Fig. 4. Scenario VTD: (a) VTD time evolution, (b) SUMO-VTD simulation with 80% of occupancy.

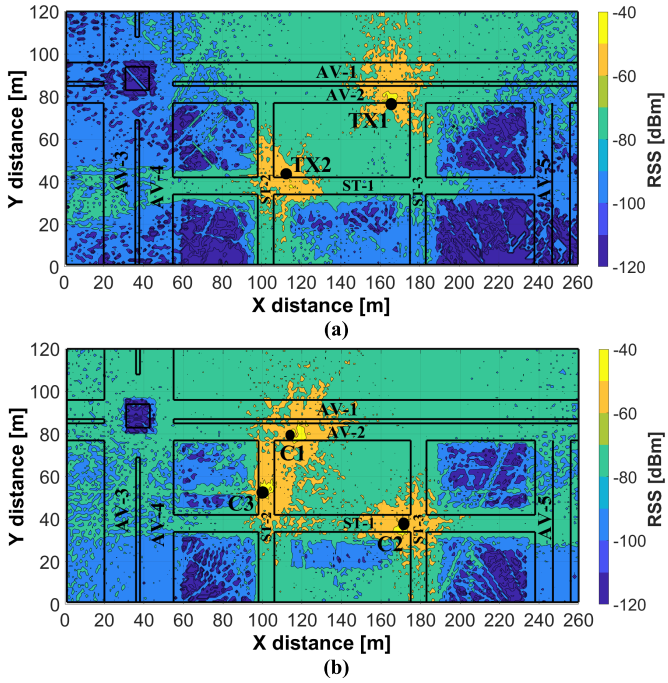

Fig. 5. HD-RSS [dBm]: (a) TX1&TX2; (b) C1&C2&C3.

A. Received Signal Strength and Spatial Path Loss

This subsection presents a detailed spatial representation of the RSS and spatial PL characterization, both as a function of the Euclidean distance TX-RX. The TX is located at a height of 3.5 m for I2V and 1.5 m height for V2V, while the RX height is 1.5 m for both. Fig. 5(a) illustrates the RSS surf-plot under HD conditions (HD-RSS) when the antennas on lamppost TX1 and TX2 (TX1&TX2) are transmitting

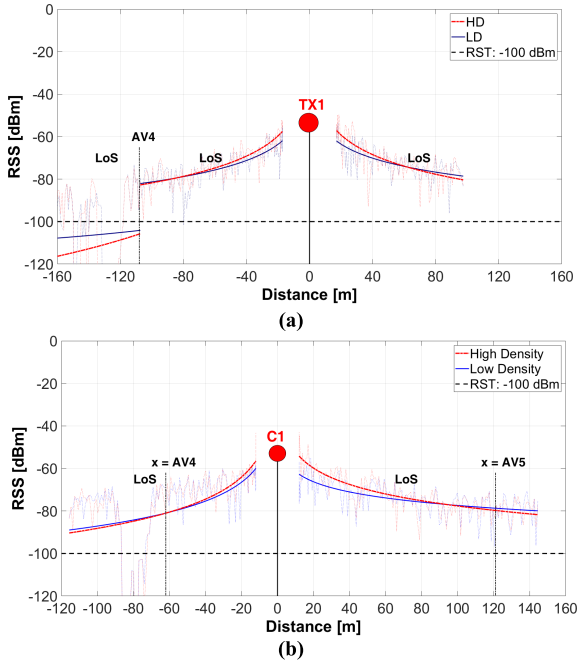

Fig. 6. RSS along AV1: (a) I2V, (b) V2V.

simultaneously, while Fig. 5(b) shows an HD-RSS surf-plot when antennas on cars C1, C2 and C3 (C1&C2&C3) are transmitting.

In Fig. 5(a), and considering definitions in Fig. 3(a), it is observed RSS values above the RST (-100 dBm) along AV-1, AV-2, ST-1, ST-2, ST3 which mean I2V coverage for these areas, whereas AV-3, AV-4, AV-5 in the roundabout area, show continuous or intermittent RSS values below the RST where the I2V connectivity is unfeasible. On the other hand, Fig. 5(b) shows higher RSS values received for V2V than the observed for I2V which means larger coverage area for V2V than V2I (e.g., the roundabout area is covered by C1). This is due to the lack of obstacles present nearby the cars, which facilitates the propagation of the radiated wave. Furthermore, the cars distribution and the fact that there are 3 transmitters instead of 2, provides such better results. The I2V case presents worse results due mainly to the vicinity of foliage and the metallic surface of the lampposts, which in this case affects greatly the radiation pattern of the employed monopoles: the metallic surface acts as a reflector and no power is radiated 'backwards'. Thus, a shadowing effect is created by the lampposts, reducing the coverage of these nodes.

A more detailed analysis of the RSS along AV-1, under HD and LD conditions, is depicted in Fig. 6. The large-scale spatial PL for I2V and V2V is depicted in Fig. 6(a) and Fig. 6(b) respectively. From I2V and V2V figures, it is observed higher RSS values for HD than LD in the nearer area of the TX, (approximately up to 30 m); far from this distance there are not observable differences.

The placement of the TX has great influence on the creation of the LoS, NLoS and QLoS conditions. For I2V, the path loss exponent (PLE) ranges from [2.0 - 3.3] and the standard deviation (STD) from [5.4 - 22.5] dB under

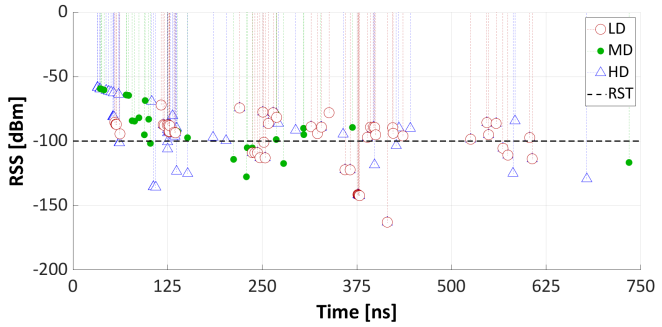

Fig. 7. V2V- PDP under 3 VTD levels.

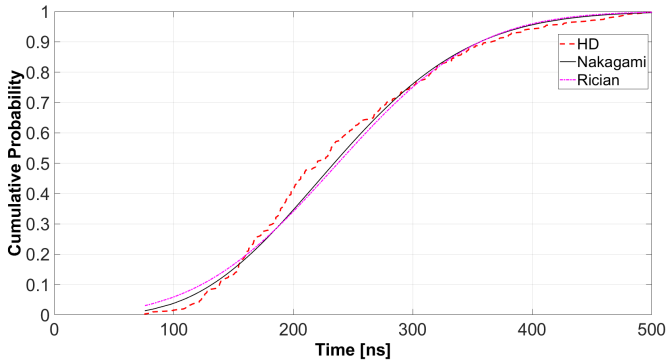

Fig. 8. V2V τ_{rms} for HD.

LoS /QLoS conditions, while the PLE varies from [3.6 - 4.3] and the STD from [38.0 - 43.0] dB under NLoS conditions. Places such as roundabout and intersections deteriorate the RSS irrespective of distance, and buildings generate high PL and notorious fluctuations. A corridor configuration at streets ST-1 and ST-2 causes the waveguide effect when roadside unit (RSU) rays impacts upon the lining walls of the buildings. For V2V, the PLE and STD values are variable, according to the temporal and spatial position of the transmitting vehicles.

B. Multipath Metrics: PDP, τ_{rms}, Doppler Shift

The PDP quantifies the number and severity of power rays in the wireless channel and is used to calculate various multipath statistics as τ_{mean}, τ_{rms}, maximum excess delay, and CB. Fig. 7 illustrates the V2V PDP at C4 when C1 (see Table II for reference) is transmitting under 3 different VTD levels. A selected timespan of 750 ns shows a highly dispersive scenario, where many power rays arrive to C4 resulting in reflected, refracted, and diffracted rays. The first ray arrives at 20 ns due to the vicinity with the transmitter.

The highest density of rays that arrives to C4 above the RST corresponds to HD, which suggests that high vehicular densities are related to high dispersive effects and high RSS values for V2V links. This would be caused by the increase in the reflected rays that impact on the metallic roof of the cars and its contribution to the total RSS. Conversely, the lowest density of rays corresponds to LD. Additional simulations for locations far from the transmitter (more than 30 m) do not show significant PDP variations under different VTD.

Fig. 8 shows the τ_{rms} Cumulative Distribution Function (CDF), when C1 is transmitting (HD), along AV-1 (a segment

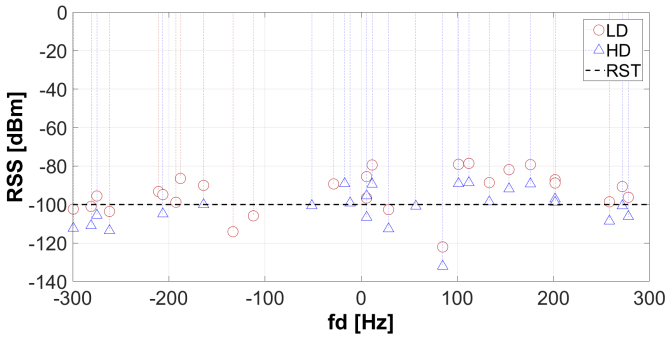

Fig. 9. I2V- Doppler shift under 2 different VTD levels.

TABLE V
I2V-DOPPLER SHIFT (WHEN TX1 IS TRANSMITTING)

C4 relative velocity [km/h]	Theoretical positive/negative fd_{max} offset [Hz]	3D-RL positive fd_{max} offset [Hz]	3D-RL negative fd_{max} offset [Hz]
60	327.78	278.00	300.00
40	218.51	215.00	205.00

of 15 m left to C1). It is observed a good fit with Nakagami or Rician distribution, commonly used to describe the fast fading channel delay dispersion. The mean τ_{rms} value is approximately 250 ns. Additional simulation shows a good agreement with Lognormal distribution. Authors in [48], propose the use of a mixture of Rayleigh and Rician distributions to characterize the τ_{rms} under conditions of LoS and NLoS.

The time-varying nature of the channel caused by the relative motion between the mobile and base station in the small-scale region can be described by the Doppler spread (D_S) and coherence time (T_C). D_S is defined as the range of frequencies over which the received Doppler spectrum is essentially non-zero. Doppler shift (fd) is the Doppler spectrum of the received signal in the range fc – fd to fc + fd, where fc is the transmit frequency [44]. Fig. 9 depicts the I2V-Doppler shift at C4, under 2 different VTD levels, when TX1 is transmitting. C4 is traveling at a constant velocity of 60 km/h. Although there are variations in the frequency components of the Doppler, the f_{dmax} (positive and negative) remains approximately equal for LD and HD while, it is observed from Fig. 7 and Fig. 9, more evenly distributed PDP and Doppler taps under HD.

The theoretical maximum Doppler shift, fd_{max}, for a transmission frequency of 5.9 GHz, when $\cos\theta = 1$ (θ is the angle between the direction of motion of the mobile and direction of arrival of scattered waves) is $f_{dmax}(60\text{ km/h}) = 327.78$ Hz. According to 3D-RL results, the received signal spectrum will have components in the range $f_{60\text{km/h}} = (5.9 \times 10^9 - 300.0$ to $5.9 \times 10^9 + 278.0)$ Hz; additional simulation for 40 km/h where performed and the results are summarized in Table V.

IV. STATISTICAL ANALYSIS

The identification of the statistical fading model that fits and characterizes the fading level of this multipath scenario is required, as well as the adoption of descriptive statistics to measure it. Different fading models such as Gamma,

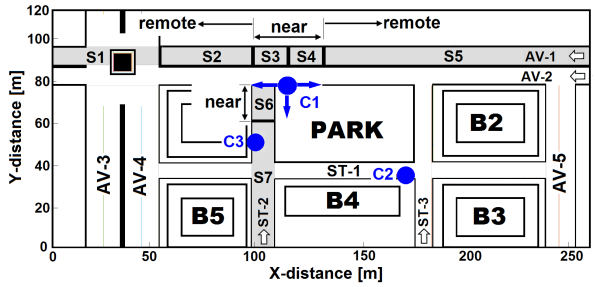

Fig. 10. Scenario segmentation for V2V analysis when C1 is transmitting.

Lognormal, Rician [25], Rayleigh, Nakagami, Weibull; composite fading models as Weibull-Gamma [49], Nakagami-Lognormal, *K* distribution (mixture of Rayleigh and Gamma); mixtures of Gamma distributions [50], etc., have been proposed and utilized to characterize the fading channel in vehicular environments that change over distance, time, and mobility. To measure the closeness of the data with the theoretical distributions, graphical and descriptive statistical tools are used. Graphical tools such as probability plot (pp-plot) which keeps similarity with the quantile-to-quantile plot analysis [51], and descriptive tools as goodness-of-fit (GOF) and squared coefficient of variation (SCV).

To measure the GOF of the resulting non-parametric RSS 3D-RL data with some theoretical distributions, the Anderson-Darling (AD) test with 5.0% for the significance level of the hypothesis (H_0) test is used. The AD statistic provides robustness and flexibility because it gives heavyweight to the tails and should be powerful against alternatives in which the true distribution and the data disagree near the tails of the data distribution. AD has been employed to quantify the difference between the observed and expected values [52], as a type of divergence or discrepancy measurement. To measure the differences between CDF's resulted of the different I2V-VTD or V2V-VTD test, a one-side Kolmogorov-Smirnov (K-S) test was performed at 5.0% for the significance level of the hypothesis (H_0). To measure the data variability, the SCV was used [53]. Indeed, the SCV characterizes the amount of fading (AF) of the received signal power, [42].

For statistical analysis, symmetric and equidistant data segments from TX were selected, S1 to S5 along AV-1 and S6 to S7 along ST-2, as is depicted in Fig. 10, to have as much as possible, consistent data for GOF analysis.

This kind of segmentation was chosen for four reasons: a) to identify the spatial differences between symmetric and equidistant areas from TX (C1), b) to organize the 3D-RL RSS data into homogeneous segments, avoiding extreme values, c) to group segments under similar LoS, QLoS or NLoS criteria and d) to identify near areas to the TX (up to 30 m) which are characterized by high data variability. Data segments in the vicinity should be shorter than in remote locations.

Fig. 11 shows the V2V-RSS pp-plot of two segments along AV-1: the segment S3 and the joint segment S1-S2-S3 (S1-S3) when C1 is transmitting. The RSS data were plotted against a theoretical Lognormal distribution which is represented by the black-dotted straight line; departure from the straight line indicates departure from the specified distribution.

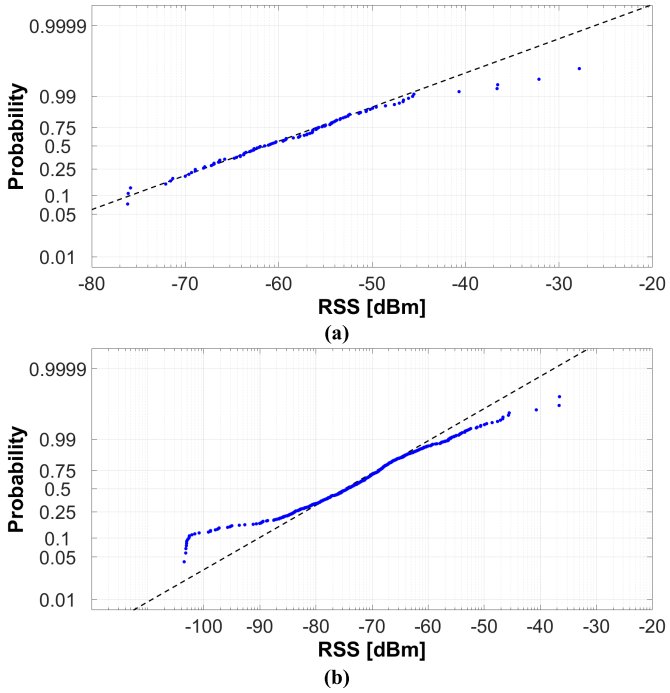

Fig. 11. RSS pp-plot: (a) S3 vs Lognormal distribution, (b) S1-S3 vs Lognormal Distribution.

From Fig. 11(a), it is observed that S3-RSS data lie closer to the straight line with some departure from the right-sided tail which could be caused by the natural variation in the RSS (outliers). This graphical result suggests a good fit between the S3-RSS data and the proposed distribution; in other words, the S3-RSS behavior would be characterized by a Lognormal distribution. Conversely, Fig. 11(b) shows that the S1-S3 RSS data departs from the straight line, mainly at the right-sided and left-sided tails, which is an indicator that the S1-S3 RSS do not follow the proposed distribution. This lack of fit could be caused by the high data variability in the analyzed segment. Additional pp-plot analysis for Exponential, Rician and Lognormal distributions for S1-S3 and S6-S7 segments, resulted in a similar departure of the RSS data to those distributions. These results give insight into the necessity to evaluate individual segments and define metrics to find the statistical distribution able to represent the RSS data.

Fig. 12 depicts the graphical GOF between the RSS and some distributions used in the description of multipath fading environments as Gamma, Lognormal, Nakagami, and Weibull. Fig. 12(a) depicts the comparison between the Empirical Cumulative Distribution Function (ECDF) of S3-RSS (under HD) and the aforementioned distributions, where the best fit is observed for the lognormal distribution, which is confirmed with the AD-GOF analysis presented in Table VI (item c), with the non-rejection of the null hypothesis (H_0 is False). Table VI additionally summarizes the SCV, the AD-GOF test with 5.0% for a significance level of the hypothesis (H_0), the AD statistics as a measure of divergence and, the input parameter (shape) for the tested distributions.

There are segments such as S2 and S6, that were fitted by more than one distribution, however, the best fit is defined by the smallest "AD-value" given that this statistic

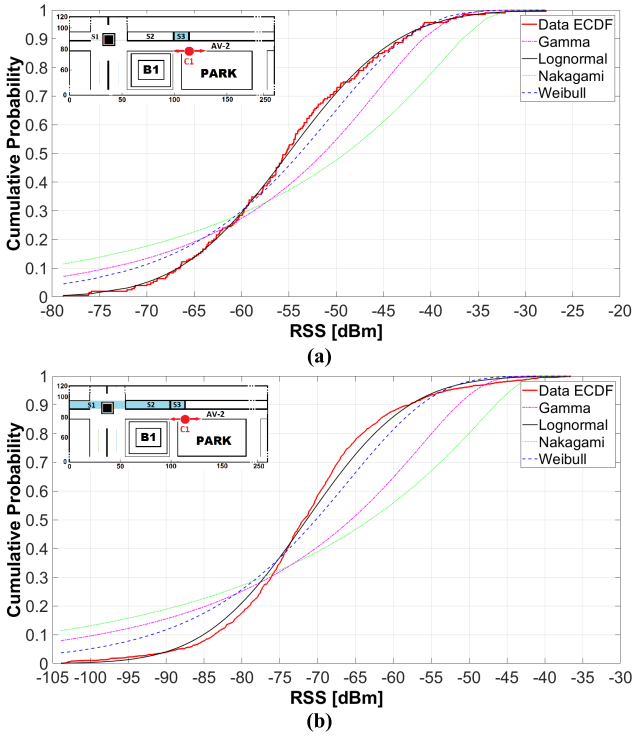

Fig. 12. ECDF-GOF: (a) S3-RSS, (b) S1-S3 RSS.

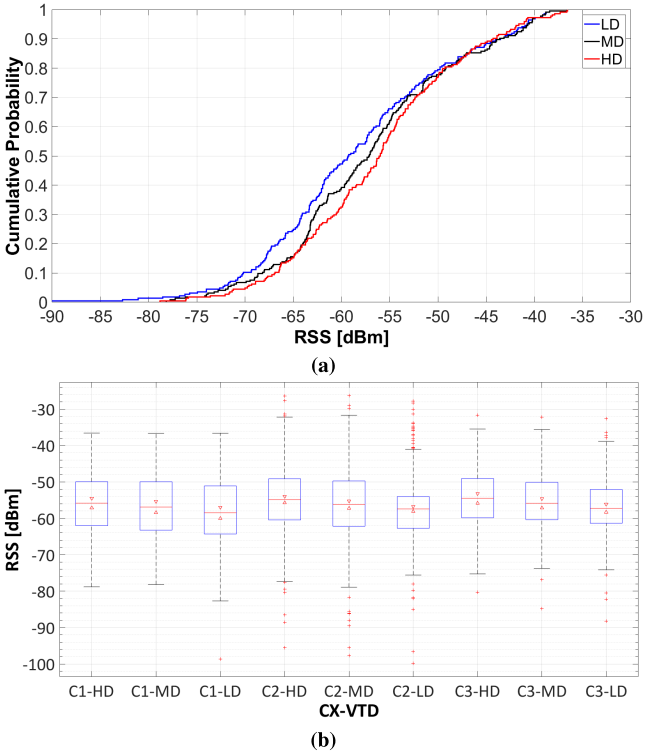

Fig. 13. RSS VTD effect: (a) ECDF- GOF for S3, (b) boxplot analysis for C1, C2, C3.

TABLE VI
DATA DISPERSION MEASUREMENTS AND GOF TEST FOR C1

Segment	SCV	Lg.	Gm.	Nk.	Wb.
a) S1 (60 m)					
AD-GOF (H/S)	1.95	T /10.02	F /1.22	T /12.58	F /0.39
Shape factor		2.92	0.67	0.24	0.76
b) S2 (100 m)					
AD-GOF (H/S)	1.96	T /2.92	T /2.97	T /19.57	F /2.09
Shape factor		4.83	0.86	0.28	0.87
c) S3 (20 m)					
AD-GOF (H/S)	6.03	F /1.06	T /2.98	T /13.79	F /0.87
Shape factor		6.37	0.53	0.18	0.65
d) S1-S3 (120 m)					
AD-GOF (H/S)	23.77	T /3.12	T /Inf	T /Inf	T /18.87
Shape factor		4.13	0.35	0.11	0.51
e) S6 (20 m)					
AD-GOF (H/S)	1.57	T /8.65	F /1.23	T /13.45	F /0.71
Shape factor		3.59	0.74	0.28	0.85
f) S7 (60 m)					
AD-GOF (H/S)	2.86	T /2.91	F /2.34	T /12.29	F /0.94
Shape factor		5.65	0.63	0.22	0.72
g) S6-S7 (80 m)					
AD-GOF (H/S)	7.31	F /2.09	T /37.14	T /inf	T /13.44
Shape factor		4.25	0.44	0.15	0.58

AD-GOF (H / S) = Anderson-Darling GOF (Hypothesis test / statistic test)
SCV = Squared Coefficient of Variation.
Lg = Lognormal, Gm = Gamma, Nk = Nakagami, Wb = Weibull.
T / F = True / False (for hypothesis test validation)

can be considered a divergent or discrepant measurement, [55] (e.g., for S6 the best fit corresponds to Weibull distribution). From Fig. 12(b), it is observed an approximate fit between S1-S3 ECDF and Lognormal distribution, however, Table VI (item d) shows the rejection of the null hypothesis with all the tested distributions. The length and high data variability of this segment expressed by the SCV value would be a factor that causes this lack of fit.

For practical purposes, even though the segment S1-S3 cannot be described, under stringent statistical sense, by anyone of the tested distribution, nonetheless, it would be "fitted" by a Lognormal distribution given its smaller AD-statistic. Additional segments as S1, S2, S3, S5, S6, S7 and S5, S6 (not registered in Table VI) can be described in terms of Lognormal or Weibull distributions. It is worth noting that the SCV of each segment is significantly smaller than the SCV of joint segments which ease the statistical fitting. The input parameter (shape), estimated from the 3D-RL RSS data that characterizes the distributions, is not constant, showing variations according to the length and position to the TX. These results give an insight that the shape factor is variable depending on the scenario characteristics, as it is the PLE, which must be considered for further simulations.

Fig. 13 illustrates the effect of the VTD in the RSS. Fig. 13(a) shows the S3-RSS ECDF under HD, MD, and LD when C1 is transmitting. It is observed that higher values of RSS are related to HD and lower values to LD. The 0.5 cumulative probability is approximately -56 dBm for HD, -58 dBm for MD and -60 dBm for LD. A performed one-side K-S test at 5.0% for a significance level, showed significant differences between HD and LD (HD resulted "smaller" than LD). The K-S test between HD and MD or MD and LD did not show significant differences. Additional one-side K-S test for S1, S2, S5, S7 did not show significant differences when comparing HD, MD and LD.

These results are in concordance with those observed in Fig. 6(b) and suggest that HD conditions have impact in the V2V RSS values of the segments located near the transmitter while no significant impact is evidenced for segments located in remote areas (see Fig. 10 for reference).

TABLE VII
V2V-RSS STATISTICS FOR SEGMENTS NEAR TO C1, C2, C3

CX-VTD	Q1 [dBm]	Q2 [dBm]	Q3 [dBm]	STD [dB]	SCV
C1 – HD	-62.02	-55.80	-49.92	18.80	5.25
C1 – MD	-63.24	-56.90	-49.95	20.60	4.45
C1 – LD	-64.30	-58.45	-51.09	19.60	4.86
C2 – HD	-60.43	-54.84	-49.12	20.66	18.22
C2 – MD	-62.18	-56.20	-49.72	20.83	18.56
C2 – LD	-62.72	-57.42	-54.01	23.01	24.63
C3 – HD	-59.83	-54.50	-49.06	29.00	8.94
C3 – MD	-60.37	-55.86	-50.09	29.33	12.77
C3 – LD	-61.35	-57.21	-52.07	30.87	24.63

Q1 = Quartile1 (25%), Q2 = Quartile2 (50%), Q3 = Quartile3 (75%)

TABLE VIII
V2V-RSS STATISTICS FOR SEGMENTS REMOTE TO C1, C2, C3

CX-VTD	Q1 [dBm]	Q2 [dBm]	Q3 [dBm]	STD [dB]	SCV
C1 – HD	-75.36	-70.92	-67.53	51.05	2.11
C1 – MD	-74.67	-70.32	-66.92	57.62	1.27
C1 – LD	-74.97	-70.66	-67.09	52.53	1.30
C2 – HD	-77.05	-72.75	-69.15	15.11	1.89
C2 – MD	-76.90	-73.31	-69.95	15.89	1.76
C2 – LD	-76.86	-72.88	-69.31	15.80	1.97
C3 – HD	-66.96	-63.71	-60.91	29.83	1.01
C3 – MD	-68.47	-64.56	-61.34	25.79	2.87
C3 – LD	-68.251	-64.74	-62.01	29.82	1.97

To confirm the results, the effect of the VTD for V2V was analyzed for two additional transmitters, C2 and C3, for segments located in their vicinity (analogous to S3, S4, S5 when C1 is transmitting). Fig. 13(b) depicts the RSS boxplot when C1, C2 or C3 is transmitting under HD, MD, and LD. It is observed difference and trend mainly for the median RSS of each transmitter, where HD keeps correspondence with higher median RSS values while LD is related to lower median RSS values. The interquartile range remains constant for C1 and C3 while some variation is reported for C2-MD, possibly due to a specific car distribution in the scenario.

Table VII and Table VIII show more detailed RSS statistic measurements as quartile values (25%, 50%, 75%), STD and SCV, of near and remote areas of C1, C2, C3, respectively, under different VTD levels. From Table VII the most noticeable difference corresponds to the second quartile (Q2) - the median of the RSS data - where higher RSS values are related to higher VTD levels. There is approximately a 3 dB difference between C3-HD and C3-LD. The first quartile (Q1) and third quartile (Q3) show an analogous trend as Q2. Measures as STD and SCV do not show apparent RSS tendency when different VTD values are compared.

For remote areas, there are no significant differences or trends in the RSS values due to the influence of the VTD, as it is described by the RSS statistics from Table VIII. The SCV indicates less data variability than remote areas.

To analyze the effect of the VTD into the V2I links, three cars have been considered, C1, C2, C3, as transmitters and three antennas on lampposts TX1, TX2, TX3 as receivers

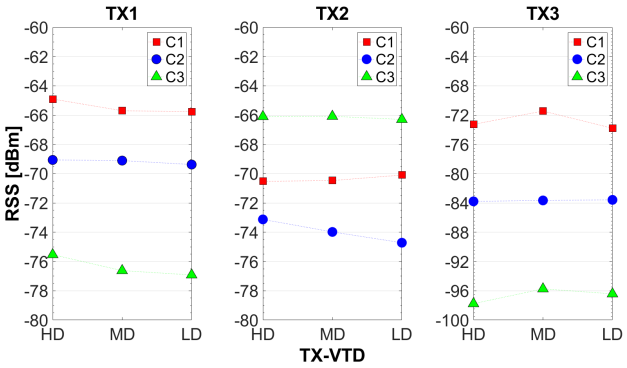

Fig. 14. I2V RSS under three VTD levels.

(see Fig. 3(a) for reference). Fig. 14 shows the mean RSS of TX1, TX2, TX3 under three different VTD levels. Factors as distance and obstacles in the LoS causes lower TX3-RSS than TX1 or TX2 RSS for all the VTD levels. Otherwise, although C3 is nearest to TX3, its RSS is below than C1 or C2, due to the significant obstruction of building 1 (B1).

From the analysis and comparison between TX1, TX2 and, TX3, there are no significant differences in the mean RSS nor some trend is observable under different VTD levels. These results suggest that V2I links are less affected by VTD.

V. MEASUREMENT CAMPAIGN

A measurement campaign has been performed in the real scenario of Plaza Gongora, in Pamplona, Spain, to validate the proposed simulation algorithm. Real pictures of the scenario are presented in Fig. 15, where the deployment of the employed equipment can be seen, as well as the surroundings of the deployed antennas. A common business day at the early morning with medium vehicles density (MD) has been chosen for the development of the measurement campaign. Two different positions for the transmitter antenna has been selected, the first one with the transmitter placed in a lamppost at 3.5 m height (same position as TX1) and the second one with the transmitter placed on the top of a vehicle at 1.5 m height (same position as C1), see Fig. 15a and Fig. 15e respectively. Fig. 4a and Table III present the reference positions of TX1 and C1.

The transmitter antenna TX was connected to a signal generator at 5.9 GHz frequency, while the receiver antenna was placed on a top of a sedan-car vehicle at 1.5 m height. The TX and RX antennas were ACA-4HSRPP-2458 from ACKme Networks, both omnidirectional, with a gain of 3.7 dB. The employed signal generator was a portable N1996A unit, from Keysight Technologies, and the spectrum analyzer was a Keysight N9912 Field Fox. Measurements were performed with 100 MHz bandwidth at 5.9 GHz frequency with a measurement time at each point of 60 seconds. The RSS at each point is the highest peak (Max-Hold function) of power shown by the spectrum analyzer, in order to compare with equivalent continuous wave operation provided by the 3D-RL simulation code. Note that for the measurements with the antenna mounted on the vehicle, one of the two lanes of the road was blocked by our car.

Regarding the radio propagation conditions of the presented measurements, Fig. 15b and Fig. 15c show the scenario under

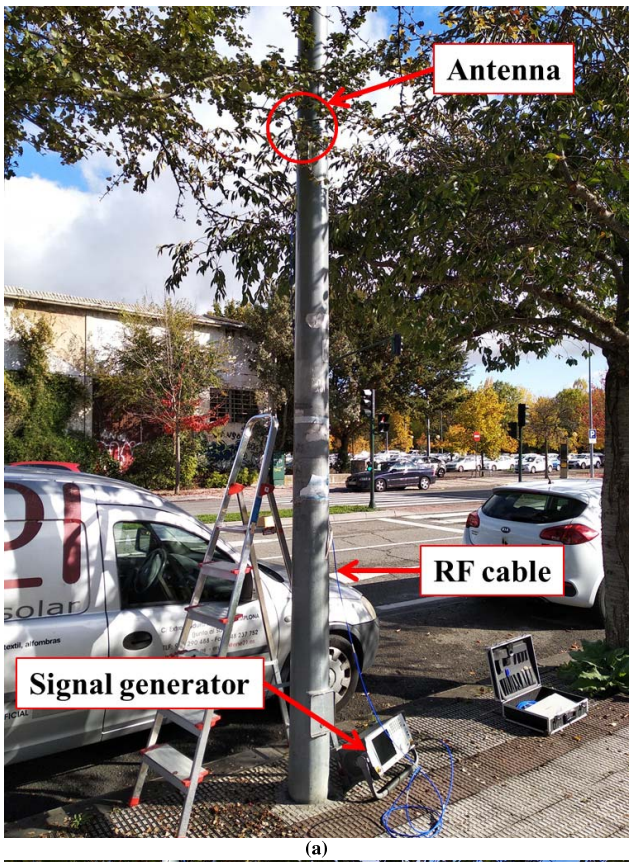

(a)

(b)

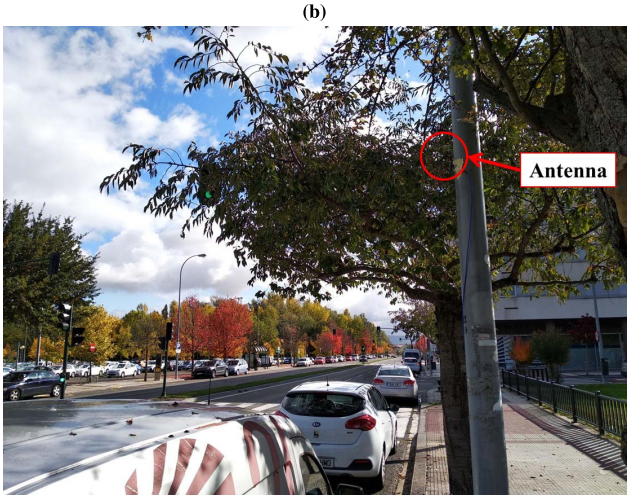

(c)

(d)

(e)

Fig. 15. Real pictures of the equipment deployment: (a) Deployment on a lamppost; (b) Left hand view of the scenario under analysis, (c) Right hand view of the scenario under analysis; (d) Detail of the deployed antenna; (e) Deployment on a conventional car.

analysis, where apart from lampposts, several trees are present in the sidewalk (with foliage nearby the transmitting antenna), as well as a lot of parked cars. These conditions make the environment very complex in terms of radio propagation, although most of the cases are LoS cases. Furthermore, as can be seen in Fig. 15d, the antenna is very close to the metallic surface of the lamppost. This fact can affect the impedance of the antenna, and therefore, worsen the radiating characteristics of the antenna.

Measurements were performed along AV-1 and AV-2 considering the lane segment between C1 to TX1 (See Fig. 3(a) for reference). Fig. 16 illustrates the RSS comparison (measurements versus 3D-RL simulation) when TX1 is transmitting (Fig. 16a) and when C1 is transmitting (Fig. 16b) versus the distance for each transmitter, respectively. Note that AV-1 is the further away avenue from both transmitter positions.

Fig. 16 shows a good agreement between 20 measured and its correspondent simulated spatial points for both transmitter positions. For the transmitter TX1, the mean error between simulation and experimental measurements is 2.71 dB (5.22 dB STD) and 2.06 dB (3.07 dB STD) for AV-1 and AV-2 respectively. The largest RSS variations are observed in the

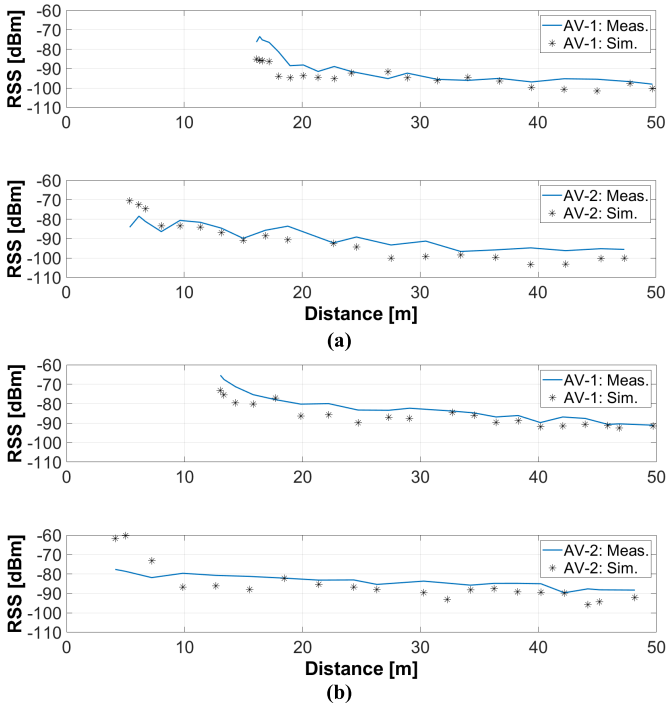

* Meas: field measurements, Sim: 3D-RL simulation

Fig. 16. RSS measurements vs simulation comparison: (a) when TX1 is transmitting, (b) when C1 is transmitting.

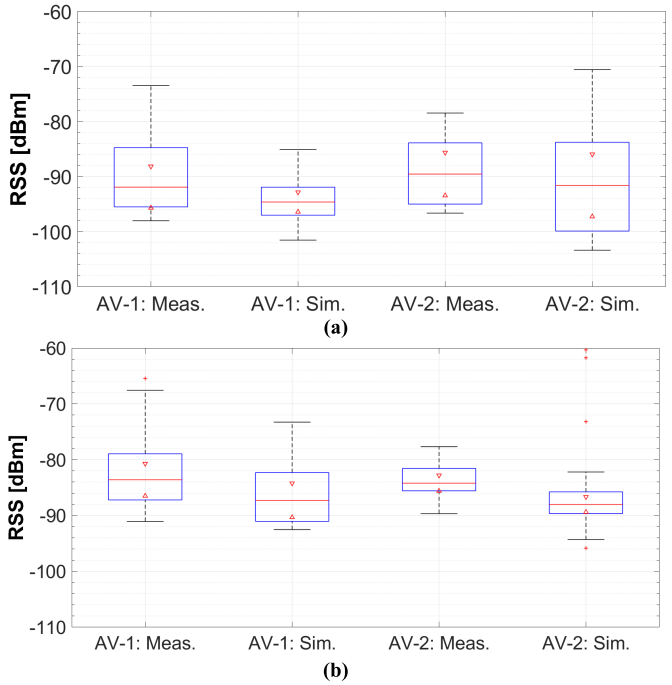

* Meas: field measurements, Sim: 3D-RL simulation

Fig. 17. RSS BoxPlot measurements vs simulation comparison: (a) when TX1 is transmitting, (b) when C1 is transmitting.

vicinity of the transmitter, which is in concordance with the high RSS variability reported in Section III. For the transmitter C1, the mean error has been 3.68 dB (3.45 dB STD) and 3.82 dB (4.50 dB STD) for AV-1 and AV-2 respectively. Higher deviations are given mainly by the impact of antenna location in real operating conditions (with partial impedance mismatch) as well as by local variations in scenario definition in the measurement intervals under consideration.

Fig. 17 depicts the RSS boxplot when TX1 and C1 are transmitting under MD. It is observed for both transmitter cases that the interquartile range remains constant for AV-1 and AV-2. It can be noticed that some extreme values are observed for AV-2-Sim in the C1 transmitter case, possibly due to a specific car distribution in the scenario because in this case, the transmitter and receiver are at the same height. Mean differences between the compared values are more notorious for C1 than TX1 which keep concordance with the results obtained in Sections III and IV where it is observed an increase in the SCV for C1 transmission mainly in the vicinity of the transmitter.

VI. Conclusion

In this work, the characterization of the impact of the VTD into the URPC for V2X channels has been presented. The use of integrated computational tools such as a geographic database, a deterministic 3D-RL algorithm, and a microscopic vehicular simulator, has been presented in detail. The integration process has been implemented, based on the sequential exchange of information between VTD, 3D-RL and network simulation block, in order to enable further data analysis. The solution methodology considers 3 different VTD levels whose impact into the V2X links is analyzed through statistical measurements and presented for large-scale and small-scale metrics. The resulted volumetric PDP and τ_{rms} provide insight into coverage and capacity ratios, adaptive modulation parameterization, equalization requirements, and coding schemes.

In order to obtain consistent and homogeneous data for RSS analysis and statistical measurement, considerations as the spatial distance (near and remote), symmetry, and equidistance from TX are required. The GOF analysis shows that Log-normal and Weibull distributions can characterize the V2X-RSS for HD, MD and LD where Weibull distribution best-fit individual/small data segments, while jointly/large segments are best represented by Lognormal distribution.

Statistical metrics suggest VTD affectation to the mean RSS in near areas of the TX. Thereby, for V2V and I2V links HD induces the highest RSS values while LD is related to the lowest RSS values. This could be caused by the increase in the reflected rays that impact on the metallic roof of the cars and its contribution to the total RSS. For remote areas from TX, there were not reported significant differences for V2V and I2V. On the other hand, the results suggest that Doppler taps tend to be more evenly distributed across all Doppler frequencies with a higher VTD with some variations in the frequency components of the apparent received frequency. The maximum Doppler shift is relatively similar for different levels of VTD.

As future work, the identification of other significant parameters (i.e. different car type, vehicular distribution, QLoS conditions, etc.) or specific environmental variables, as well as different frequency bands is currently under consideration in order to obtain a more accurate channel characterization in these complex environments. The consideration of variable

scatterers within time domain with focus on reducing computational complexity is also foreseen.

ACKNOWLEDGMENT

The traffic mobility files were generated using traffic simulator SUMO.

REFERENCES

[1] University of Michigan. *Transportation Research Institute-ITS Publications*. Accessed: Feb. 4, 2017. [Online]. Available: http://www.umtri.umich.edu/our-focus/intelligent-transportation-systems

[2] WAYMO. *Technology-We're Building a Safer Driver That is Always Alert and Never Distracted*. Accessed: Apr. 30, 2018. [Online]. Available: https://waymo.com/tech/

[3] World Bank Group. *Intelligent Transport Systems—Toolkit for European Union*. Accessed: Apr. 30, 2018. [Online]. Available: https://ppp.worldbank.org/public-private-partnership/library/intelligent-transport-systems-its-toolkit-european-union.

[4] *Part 11: Wireless LAN Medium Access Control (MAC) and Physical Layer (PHY). Specifications-Amendment 6: Wireless Access in Vehicular Environments*, Standard IEEE Std 802.11: 2010, New York, NY, USA, USA, 2010.

[5] *IEEE Standard for Wireless Access in Vehicular Environments (WAVE)–Multi-Channel Operation*, IEEE Standard 1609.4-2016, New York, NY, USA, 2016.

[6] K. A. Hafeez, L. Zhao, B. Ma, and J. W. Mark, "Performance analysis and enhancement of the DSRC for VANET's safety applications," *IEEE Trans. Veh. Technol.*, vol. 62, no. 7, pp. 3069–3083, Sep. 2013.

[7] V. Tyagi, S. Kalyanaraman, and R. Krishnapuram, "Vehicular traffic density state estimation based on cumulative road acoustics," *IEEE Trans. Intell. Transp. Syst.*, vol. 13, no. 3, pp. 1156–1166, Sep. 2012.

[8] L. Liang, H. Peng, G. Y. Li, and X. Shen, "Vehicular communications: A physical layer perspective," *IEEE Trans. Veh. Technol.*, vol. 66, no. 12, pp. 10647–10659, Dec. 2017.

[9] N. Dreyer, A. Moeller, J. Baumgarten, Z. H. Mir, T. Kuerner, and F. Filali, "On building realistic reference scenarios for IEEE 802.11p/LTE-based vehicular network evaluations," in *Proc. IEEE 87th Veh. Technol. Conf. (VTC Spring)*, Jun. 2018, pp. 1–7.

[10] J. Gozalvez, M. Sepulcre, and R. Bauza, "IEEE 802.11p vehicle to infrastructure communications in urban environments," *IEEE Commun. Mag.*, vol. 50, no. 5, pp. 176–183, May 2012.

[11] C.-X. Wang, A. Ghazal, B. Ai, Y. Liu, and P. Fan, "Channel measurements and models for high-speed train communication systems: A survey," *IEEE Commun. Surveys Tuts.*, vol. 18, no. 2, pp. 974–987, 2nd Quart., 2016.

[12] D. W. Matolak and A. Chandrasekaran, "5 GHz intra-vehicle channel characterization," in *Proc. IEEE Veh. Technol. Conf. (VTC Fall)*, Sep. 2012, pp. 1–5.

[13] L. Azpilicueta *et al.*, "Characterization of wireless channel impact on wireless sensor network performance in public transportation buses," *IEEE Trans. Intell. Transp. Syst.*, vol. 16, no. 6, pp. 3280–3293, Dec. 2015.

[14] M. Boban, J. Barros, and O. K. Tonguz, "Geometry-based vehicle-to-vehicle channel modeling for large-scale simulation," *IEEE Trans. Veh. Technol.*, vol. 63, no. 9, pp. 4146–4164, Nov. 2014.

[15] F. Granda *et al.*, "Spatial characterization of radio propagation channel in urban vehicle-to-infrastructure environments to support WSNs deployment," *Sensors*, vol. 17, no. 6, p. 1313, Jun. 2017.

[16] E. Tan and J. Chen, "Vehicular traffic density estimation via statistical methods with automated state learning," in *Proc. IEEE Conf. Adv. Video Signal Based Surveill.*, Sep. 2007, pp. 164–169.

[17] C.-x. Wang, X. Cheng, and D. Laurenson, "Vehicle-to-vehicle channel modeling and measurements: Recent advances and future challenges," *IEEE Commun. Mag.*, vol. 47, no. 11, pp. 96–103, Nov. 2009.

[18] I. Sen and D. W. Matolak, "Vehicle–vehicle channel models for the 5-GHz band," *IEEE Trans. Intell. Transp. Syst.*, vol. 9, no. 2, pp. 235–245, Jun. 2008.

[19] C. Xiang, W. Cheng-Xiang, D. Laurenson, S. Sana, and A. Vasilakos, "An adaptive geometry-based stochastic model for non-isitropic MIMO mobile-to-mobile channels," *IEEE Trans. wireless Commun.*, vol. 8, no. 9, pp. 4824–4835, Oct. 2009.

[20] C. F. Mecklenbrauker *et al.*, "Vehicular channel characterization and its implications for wireless system design and performance," *Proc. IEEE*, vol. 99, no. 7, pp. 1189–1212, Jul. 2011.

[21] I. Rashdan, M. Schmidhammer, F. de Ponte Mueller, and S. Sand, "Performance evaluation of vehicle-to-vehicle communication for cooperative collision avoidance at urban intersections," in *Proc. IEEE 86th Veh. Technol. Conf. (VTC-Fall)*, Sep. 2017, pp. 1–5.

[22] Z. Hameed Mir and F. Filali, "LTE and IEEE 802.11p for vehicular networking: A performance evaluation," *EURASIP J. Wireless Commun. Netw.*, vol. 2014, no. 1, pp. 1–15, Dec. 2014.

[23] K. Sjoberg Bilstrup, E. Uhlemann, and E. G. Strom, "Scalability issues of the MAC methods STDMA and CSMA of IEEE 802.11p when used in VANETs," in *Proc. IEEE Int. Conf. Commun. Workshops*, Cape Town, South Africa, May 2010.

[24] Institute of Transport Research (DLR). (2019). *Eclipse SUMO—Simulation of Urban MObility*. Accessed: Oct. 10, 2019. [Online]. Available: https://www.dlr.de/ts/en

[25] L. Bernado, T. Zemen, F. Tufvesson, A. F. Molisch, and C. F. Mecklenbrauker, "Time- and frequency-varying K-factor of non-stationary vehicular channels for safety-relevant scenarios," *IEEE Trans. Intell. Transp. Syst.*, vol. 16, no. 2, pp. 1007–1017, Apr. 2015.

[26] Z. Yun and M. F. Iskander, "Ray tracing for radio propagation modeling: Principles and applications," *IEEE Access*, vol. 3, pp. 1089–1100, 2015.

[27] J. S. Lu *et al.*, "A discrete environment-driven GPU-based ray launching algorithm," *IEEE Trans. Antennas Propag.*, vol. 67, no. 2, pp. 1180–1192, Feb. 2019.

[28] OSMF. (2019). *OpenStreetMap*. Accessed: Oct. 10, 2019. [Online]. Available: https://www.openstreetmap.org

[29] T. Kurner and M. Schack, "3D AC embedded into an integrated simulator for car-to-X communications," in *Proc. URSI Int. Symp. Electromagn. Theory*, Aug. 2010, pp. 880–882.

[30] J. Nuckelt, M. Schack, and T. Kürner, "Deterministic and stochastic channel models implemented in a physical layer simulator for car-to-X communications," *Adv. Radio Sci.*, vol. 9, pp. 165–171, Aug. 2011.

[31] Z. H. Mir and F. Filali, "Simulation and performance evaluation of vehicle-to-vehicle (V2V) propagation model in urban environment," in *Proc. 7th Int. Conf. Intell. Syst., Modeling Simulation (ISMS)*, Jan. 2016, pp. 394–399.

[32] J. Harri, F. Filali, and C. Bonnet, "Mobility models for vehicular ad hoc networks: A survey and taxonomy," *IEEE Commun. Surveys Tuts.*, vol. 11, no. 4, pp. 19–41, 4th Quart., 2009.

[33] S. Salous, *Radio Propagation Measurement and Channel Modelling*, 1st ed. London, U.K.: Wiley, 2013.

[34] S. Loredo, A. Rodriguez-Alonso, and R. P. Torres, "Indoor MIMO channel modeling by rigorous GO/UTD-based ray tracing," *IEEE Trans. Veh. Technol.*, vol. 57, no. 2, pp. 680–692, Mar. 2008.

[35] (2019). *JOSM*. Accessed: Oct. 10, 2019. [Online]. Available: https://josm.openstreetmap.de/

[36] M. Haklay and P. Weber, "OpenstreetMap: User-generated street maps," *IEEE Pervas. Comput.*, vol. 7, no. 4, pp. 12–18, Oct. 2008.

[37] S. Krauß, "Microscopic modeling of traffic flow: Investigation of collision free vehicle dynamics," Univ. Cologne, Cologne, Germany, Tech. Rep. DLR-FB-98-08, 1998.

[38] P. G. Gipps, "A behavioural car-following model for computer simulation," *Transp. Res. B, Methodol.*, vol. 15, no. 2, pp. 105–111, Apr. 1981.

[39] W. M. Griggs, R. H. Ordonez-Hurtado, E. Crisostomi, F. Hausler, K. Massow, and R. N. Shorten, "A large-scale SUMO-based emulation platform," *IEEE Trans. Intell. Transp. Syst.*, vol. 16, no. 6, pp. 3050–3059, May 2015.

[40] B. Aygun, M. Boban, J. P. Vilela, and A. M. Wyglinski, "Geometry-based propagation modeling and simulation of vehicle-to-infrastructure links," in *Proc. IEEE 83rd Veh. Technol. Conf. (VTC Spring)*, May 2016, pp. 3–7.

[41] GNI Insurance Agency. *World Geodetic System 1984 (WGS 84)*. Accessed: Jun. 18, 2018. [Online]. Available: https://www.nga.mil/ProductsServices/GeodesyandGeophysics/Pages/WorldGeodeticSystem.aspx

[42] R. Roess, W. McShane, and E. Prassas, *Traffic Engineering*, 2nd ed. Upper Saddle River, NJ, USA: Prentice-Hall, 1998.

[43] L. Azpilicueta, *Characterization of Wireless Propagation in Complex Indoor Scenarios*. Pamplona, Spain: Universidad Pública de Navarra, 2015.

[44] T. Rappaport, *Wireless Communications: Principles and Practice*, 2nd ed. Upper Saddle River, NJ, USA: Prentice-Hall, 2002.

[45] RedPine Signals. (2018). *Driving Wireless Convergence. WaveCombo Module. 802.11p V2X*. Accessed: Feb. 28, 2018. [Online]. Available: http://www.redpinesignals.com/Products/802.11p_V2X_Connectivity/802.11p_V2X_Module.php

[46] Kapsch TrafficCom. (2018). *In-Vehicle Products (5.9 Ghz). EVK-3300. V2X Evaluation Kit*. Accessed: Feb. 28, 2018. [Online]. Available: https://www.kapsch.net/ktc/downloads/
[47] Ublox. (2018). *VERA-P1 Series. Host-Based V2X Transceiver Modules. Product Information*. Accessed: Feb. 28, 2018. [Online]. Available: https://www.u-blox.com/en/product/vera-p1-series
[48] G. A. Dimitrakopoulos and C. N. Capsalis, "Statistical modeling of RMS-delay spread under multipath fading conditions in local areas," *IEEE Trans. Veh. Technol.*, vol. 49, no. 5, pp. 1522–1528, Sep. 2000.
[49] P. S. Bithas, "Weibull-gamma composite distribution: Alternative multipath/shadowing fading model," *Electron. Lett.*, vol. 45, no. 14, p. 749, 2009.
[50] S. Atapattu, C. Tellambura, and H. Jiang, "Representation of composite fading and shadowing distributions by using mixtures of gamma distributions," in *Proc. IEEE Wireless Commun. Netw. Conf.*, Apr. 2010, pp. 1–5.
[51] NIST/SEMATECH e-Handbook of Statistical Methods. (2018). *Quantile-Quantile Plot*. Accessed: Jul. 10, 2018. [Online]. Available: https://www.itl.nist.gov/div898/handbook/eda/section3/qqplot.htm
[52] N. ur Rehman, K. Naveed, S. Ehsan, and K. McDonald-Maier, "Multi-scale image denoising based on goodness of fit (GOF) tests," in *Proc. 24th Eur. Signal Process. Conf. (EUSIPCO)*, Aug. 2016, pp. 1548–1552.
[53] H. Abdi, "Coefficient of variation," in *Encyclopedia of Research Design*, N. J. Salkind, D. M., Dougherty, and B. Frey, Eds. Newbury Park, CA, USA: Sage, 2010, pp. 169–171.
[54] U. Charash, "Reception through Nakagami Fading multipath channels with random delays," *IEEE Trans. Commun.*, vol. TCOMM-27, no. 4, pp. 645–670, Apr. 1979.
[55] E. Liebscher, "Approximation of distributions by using the anderson darling statistic," *Commun. Statist.-Theory Methods*, vol. 45, no. 22, pp. 6732–6745, Nov. 2016.

Fausto Granda (Student Member, IEEE) received the degree in electronic engineering from the Universidad de las Fuerzas Armadas ESPE, Quito, Ecuador, and the Ph.D. degree in information and telecommunications technologies from the Tecnológico de Monterrey in 2018. He is currently working as a Professor and a Researcher with the Universidad de las Fuerzas Armadas ESPE. His research interests are on vehicular networks, ray tracing and channel modeling, wireless sensor networks, and wireless system analysis.

Leyre Azpilicueta (Member, IEEE) received the degree in telecommunications engineering, the master's degree in communications, and the Ph.D. degree in telecommunication technologies from the Public University of Navarre (UPNA), Spain, 2009, 2011, and 2015, respectively. In 2010, she worked in the Research and Development Department, RFID Osés as a Radio Engineer. She is currently working as an Associate Professor and a Researcher with the Tecnologico de Monterrey, Campus Monterrey, Mexico. Her research interests are on radio propagation, mobile radio systems, ray tracing, and channel modeling. She has more than 150 contributions in relevant journals and conference publications. She was a recipient of the IEEE Antennas and Propagation Society Doctoral Research Award 2014, the Young Professors and Researchers Santander Universities 2014 Mobility Award, the ECSA 2014 Best Paper Award, the IISA 2015 Best Paper Award, the Best Ph.D. in 2016 awarded by the Colegio Oficial de Ingenieros de Telecomunicación, and the N2Women: Rising Stars in Computer Networking and Communications 2018 Award.

Mikel Celaya-Echarri (Student Member, IEEE) received the degree in computer science engineering from the Public University of Navarre (UPNA), Pamplona, Navarre, in 2011, and the M.Sc. degree in project management from UPNA in 2015. He is currently pursuing the Ph.D. degree in engineering of science with the Tecnologico de Monterrey. From 2011 to 2014, he worked as a Research and Development Engineer with Tafco Metawireless, Spain. From 2015 to 2017, he was a Visiting Assistant with the Networks and Telecommunications Research Group, Tecnologico de Monterrey, Mexico. His research lines are focus on high frequency electromagnetic dosimetry, radio frequency propagation, wireless sensor networks, project management, and computer science.

Peio Lopez-Iturri (Member, IEEE) received the degree in Telecommunications Engineering from the Public University of Navarre (UPNA), Pamplona, Navarre, in 2011, and the master's degree in communications and the Ph.D. degree in communication engineering UPNA in 2012 and 2017, respectively. He gets the 2018 Best Spanish Ph.D. thesis in Smart Cities in CAEPIA 2018 (3rd prize), sponsored by the Spanish network on research for Smart Cities CI-RTI and Sensors (ISSN 1424-8220). He is also affiliated with the Institute for Smart Cities (ISC), UPNA. He has worked in ten different public and privately funded research projects. He has more than 120 contributions in indexed international journals, book chapters, and conference contributions. His research interests include radio propagation, wireless sensor networks, electromagnetic dosimetry, modeling of radio interference sources, mobile radio systems, wireless power transfer, the IoT networks and devices, 5G communication systems, and EMI/EMC. He received the ECSA 2014 Best Paper Award and the IISA 2015 Best Paper Award.

Cesar Vargas-Rosales (Senior Member, IEEE) received the M.Sc. and Ph.D. degrees in electrical engineering (communications and signal processing) from Louisiana State University, Baton Rouge, USA. He was the Director of the Ph.D. Program in information and communications technologies with the Tecnologico de Monterrey, Campus Monterrey, from 2012 to 2016. He is a member of the Mexican National Researchers System (SNI), level II, a member of the Academy of Engineering of Mexico, and a Regular Member of the Mexican Academy of Sciences (AMC). He is currently the Leader of the Research Group on Telecommunications, Tecnologico de Monterrey. He has coauthored the book *Position Location Techniques and Applications* (Academic Press/Elsevier). His research interests are 5G, cognitive radio, MIMO systems, stochastic modeling, intrusion/anomaly detection in networks, position location, interference, routing in reconfigurable networks, and optimum receiver design. He is the IEEE Communications Society Monterrey Chapter Chair and the Faculty Advisor of the IEEE-HKN Lambda-Rho Chapter. He was also the Technical Program Chair of the IEEE Wireless Communications and Networking Conference (IEEE WCNC 2011).

Francisco Falcone (Senior Member, IEEE) received the degree in telecommunication engineering and the Ph.D. degree in communication engineering from the Universidad Pública de Navarra (UPNA), Spain, in 1999 and 2005, respectively. From February 1999 to April 2000, he was a Microwave Commissioning Engineer with Siemens-Italtel, deploying microwave access systems. From May 2000 to December 2008, he was a Radio Access Engineer with Telefónica Móviles, performing radio network planning and optimization tasks in mobile network deployment. From January 2009 to May 2009, he was a Co-Founding Member and the Director of Tafco Metawireless, a spin-off company from UPNA. He was an Assistant Lecturer with the Electrical and Electronic Engineering Department, UPNA, from February 2003 to May 2009. In June 2009, he become an Associate Professor with the EE Department, being the Department Head from January 2012 to July 2018. From January 2018 to May 2018, he was a Visiting Professor with the Kuwait College of Science and Technology, Kuwait. He is also affiliated with the Institute for Smart Cities (ISC), UPNA, which hosts around 140 researchers, currently acting as the Head of the ICT section. His research interests are related to computational electromagnetics applied to analysis of complex electromagnetic scenarios, with a focus on the analysis, design, and implementation of heterogeneous wireless networks to enable context aware environments. He has more than 500 contributions in indexed international journals, book chapters, and conference contributions. He received the CST 2003 and CST 2005 Best Paper Award, the Ph.D. Award from the Colegio Oficial de Ingenieros de Telecomunicación (COIT) in 2006, the Doctoral Award UPNA, 2010, the 1st Juan Gomez Peñalver Research Award from the Royal Academy of Engineering of Spain in 2010, the XII Talgo Innovation Award 2012, the IEEE 2014 Best Paper Award, 2014, the ECSA-3 Best Paper Award, 2016, and the ECSA-4 Best Paper Award, 2017.